Please cite this article in press as: Kurtenbach et al., Cell-Based Therapy Restores Olfactory Function in an Inducible Model of Hyposmia, Stem Cell Reports (2019), https://doi.org/10.1016/j.stemcr.2019.05.001

Stem Cell Reports
Article

ISSCR

OPEN ACCESS

Cell-Based Therapy Restores Olfactory Function in an Inducible Model of Hyposmia

Sarah Kurtenbach,[1,2] Garrett M. Goss,[1,2] Stefania Goncalves,[2] Rhea Choi,[3,4] Joshua M. Hare,[1,5] Nirupa Chaudhari,[2,4,6] and Bradley J. Goldstein[1,2,4,*]

[1]Interdisciplinary Stem Cell Institute, University of Miami Miller School of Medicine, 1501 NW 10th Avenue, Biomedical Research Building, Room 809, Miami, FL 33136, USA
[2]Department of Otolaryngology, University of Miami Miller School of Medicine, Miami, FL 33136, USA
[3]Medical Scientist Training Program, University of Miami Miller School of Medicine, Miami, FL 33136, USA
[4]Graduate Program in Neurosciences, University of Miami Miller School of Medicine, Miami, FL 33136, USA
[5]Department of Medicine, Division of Cardiology, University of Miami Miller School of Medicine, Miami, FL 33136, USA
[6]Department of Physiology and Biophysics, University of Miami Miller School of Medicine, Miami, FL 33136, USA
*Correspondence: b.goldstein4@med.miami.edu
https://doi.org/10.1016/j.stemcr.2019.05.001

SUMMARY

Stem cell-based therapies have been proposed as a strategy to replace damaged tissues, especially in the nervous system. A primary sensory modality, olfaction, is impaired in 12% of the US population, but lacks treatment options. We report here the development of a novel mouse model of inducible hyposmia and demonstrate that purified tissue-specific stem cells delivered intranasally engraft to produce olfactory neurons, achieving recovery of function. Adult mice were rendered hyposmic by conditional deletion of the ciliopathy-related IFT88 gene in the olfactory sensory neuron lineage and following experimentally induced olfactory injury, received either vehicle or stem cell infusion intranasally. Engraftment-derived olfactory neurons were identified histologically, and functional improvements were measured via electrophysiology and behavioral assay. We further explored mechanisms in culture that promote expansion of engraftment-competent adult olfactory basal progenitor cells. These findings provide a basis for translational research on propagating adult tissue-specific sensory progenitor cells and testing their therapeutic potential.

INTRODUCTION

Loss of olfaction affects millions of people in the US and remains a therapeutic challenge (Doty et al., 1984; Hoffman et al., 2016; Murphy et al., 2002). Sensorineural causes, such as age-related decline, post-viral damage, head trauma, or genetic disorders affecting olfactory neuron function, are often permanent (Doty et al., 1984; Hoffman et al., 2016; Kern et al., 2000; McIntyre et al., 2012; Paik et al., 1992; Seiden, 2004; Wrobel and Leopold, 2004). Neurogenic exhaustion is likely a common feature of many acquired anosmias, in which the normal replacement of damaged or senescent olfactory sensory neurons (OSNs) from progenitor basal cells is overwhelmed (Holbrook et al., 2005). Regardless of the specific etiology, a pathogenesis involving failures in neuronal maintenance, function, or renewal suggests that a cell-based therapy to replace neurons may be broadly effective.

The nasal olfactory epithelium (OE) houses bipolar OSNs (Figure 1) that detect odors at the epithelial surface and extend axons into the olfactory bulb. Due to their location in contact with the nasal airspace, OSNs are vulnerable to damage and cell death (Carr and Farbman, 1993). Tissue homeostasis is normally maintained by stem and progenitor cells in the basal layers of the epithelium, capable of generating new OSNs (Graziadei and Graziadei, 1979). In the mouse OE, neuropotent basal cells, specific markers for reserve and active stem cells, as well as aspects of their molecular regulation have been identified (Calof et al., 2002; Goldstein et al., 2015; Guillemot et al., 1993; Leung et al., 2007; Schwob et al., 2017; Tietjen et al., 2003). Globose basal cells (GBCs) are considered the principal pool of replicating stem cells that replenish OSNs, microvillar cells, sustentacular cells, and glands of the OE throughout life, whereas the horizontal basal cells represent a more quiescent reserve population (Fletcher et al., 2011; Huard et al., 1998; Leung et al., 2007). Single-cell transcriptional profiling defined expression of the surface receptor c-Kit as a key feature of GBCs in the sensory lineage (Fletcher et al., 2017). In addition, cultured GBCs, purified using antibody to c-KIT, have been successfully expanded as de-differentiated basal cell islands (Goldstein et al., 2016). Thus, the c-KIT (+) population of olfactory stem cells has the potential for a cell-based therapy.

Olfactory stem cell engraftment has been attempted in rats and mice (Chen et al., 2004; Goldstein et al., 1998). Yet, recovery of function has been challenging to demonstrate because regeneration of host OE following experimental injury precludes measuring the contribution of exogenous stem cells. In principle, this hurdle could be overcome by using congenitally anosmic hosts rescued with wild-type stem cells. However, such anosmic mice survive weaning poorly or have other health concerns (Brunet et al., 1996; Lehman et al., 2008). To overcome

Please cite this article in press as: Kurtenbach et al., Cell-Based Therapy Restores Olfactory Function in an Inducible Model of Hyposmia, Stem Cell Reports (2019), https://doi.org/10.1016/j.stemcr.2019.05.001

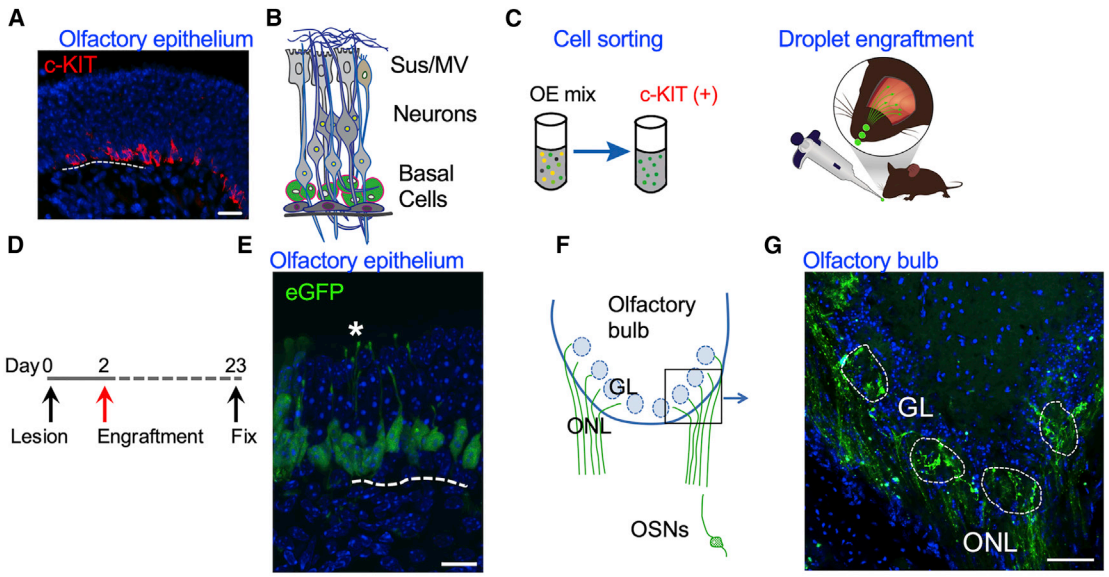

Figure 1. Neuropotent c-KIT$^+$ Basal Cells Engraft via a Simple Droplet Delivery to the Nares

(A) The c-KIT$^+$ progenitor cell population (red) resides in the basal layers of the olfactory epithelium (OE), visualized with immunolabeling. Dashed line marks the basal lamina.

(B) Organization of cell types within the OE is shown schematically: basal cells are the stem/progenitor populations, neuronal somata are located in the middle layers, and the sustentacular and microvillar (Sus/MV) cell bodies reside in the apical layer.

(C) To test engraftment potential, the c-KIT$^+$ cell fraction was purified by immunoselection from dissociated eGFP-labeled OE; cells were applied via droplet delivery to the anterior nares of wild-type mice.

(D) Experimental timeline is shown, with cells delivered 2 days following chemical olfactory lesion.

(E) Representative tissue section through the nasal region of cell-treated host; engraftment-derived eGFP$^+$ cell clusters (green) localize to the OE lining the turbinate structures and contain neurons, with dendritic knobs visible (asterisk) extending to the nasal airspace; additional imaging provided in Figure S1. Dashed line marks the basal lamina (n = 6 mice, widespread OE engraftment was evident in all subjects).

(F and G) Within the olfactory bulbs of the brain in cell-treated mice, dense layers of eGFP-labeled axons are present in the olfactory nerve layer (ONL) projecting from the nose. Anatomic organization is schematized in (F). eGFP$^+$ fibers enter glomeruli (G, outlined with dashed lines), the site of synapse with second-order neurons. GL, glomerular layer. Nuclei are stained with DAPI (blue).

Scale bars: (A) 20 μm, (E) 10 μm, (G) 100 μm.

this limitation, we have developed a genetic, inducible model of hyposmia (IH) in which GBCs yield only non-functional OSNs. Specifically, the IH mouse (c-Kit$^{CreERT2/+}$; IFT88$^{fl/fl}$), when induced, reconstitutes the OE with ciliopathic OSNs. Because olfactory receptor proteins and transduction events are normally localized to cilia, the ciliopathic neurons cannot detect odorants (Buck and Axel, 1991; McIntyre et al., 2012; Williams et al., 2014). We used this mouse model as a host for transplanting purified mouse c-KIT (+) GBCs, given their prior characterization as neuropotent stem cells (Fletcher et al., 2017; Goldstein et al., 2015). Here, we report the validation of the IH mouse model, the development of a simplified, robust cell engraftment paradigm, and demonstrate the efficacy of a cell-based therapy for olfactory loss. We show mature OSNs throughout the epithelium that are derived from engrafted cells and, importantly, demonstrate functional recovery via electrophysiology and behavioral assays.

RESULTS

Purified Adult Olfactory c-KIT (+) GBCs Are Engraftment-Competent Cells

Within the basal germinal layers of the OE, the c-KIT receptor is expressed on the surface of neuropotent GBCs (Figures 1A and 1B) (Fletcher et al., 2017; Goldstein et al., 2015; Goss et al., 2016). We have previously validated the isolation of live GBCs using immunoselection with antibody to c-KIT (Goldstein et al., 2016). To obtain large numbers of GBCs, we lesioned epithelium by injecting methimazole, which leads to cell death of mature OE and *in vivo* expansion of the GBC population (Bergman et al., 2002; Leung et al., 2007). By using available mice that express eGFP in all cells, we harvested and purified c-KIT (+) GBCs whose progeny could be traced as they colonized the regenerating epithelium. Cell engraftment was first tested by delivering cell suspension intranasally into

Please cite this article in press as: Kurtenbach et al., Cell-Based Therapy Restores Olfactory Function in an Inducible Model of Hyposmia, Stem Cell Reports (2019), https://doi.org/10.1016/j.stemcr.2019.05.001

wild-type host mice (Figures 1C and 1D). We found that 5–10 μL droplets of purified GBCs could engraft by simple delivery to the nostrils of briefly anesthetized mice over a 20–30 min period, using small volumes to prevent aspiration. Flooding the nasal fossae with cell suspension, requiring tracheotomy as reported in prior assays (Chen et al., 2004; Goldstein et al., 1998; Jang et al., 2008), was found here to be unnecessary. Histologic examination of tissue 3 weeks following engraftment revealed engraftment-derived cell clusters throughout the OE (≥5 clusters/section, n = 6 mice), identifiable by eGFP expression (Figure 1E). We considered identification of a single group of one or more eGFP-bright cells in the OE to be a "cluster" and did not attempt to draw conclusions about clonality. While auto-fluorescence from lipofuscin or other pigments can be a concern, mice treated with vehicle (no cells) revealed no evidence of the bright eGFP signal. The presence of donor-derived OSNs was readily evident by their morphology, with somata in the middle layers of the pseudostratified OE and apical dendrites ending in dendritic knobs (Figure 1E). Moreover, sections through the olfactory bulb revealed the presence of eGFP-labeled axons in the olfactory nerve layers, which contain the fibers of OSNs projecting from the OE (Figures 1F and 1G). Labeled axons could be seen entering the glomerular layer, consistent with innervation by engraftment-derived OSNs. These initial transplant studies confirm that the c-KIT (+) GBCs can engraft into the OE to produce OSNs.

Development of an Inducible Hyposmia Mouse Model

Existing syndromic or congenitally anosmic mice are undesirable transplant hosts because they have other systemic problems (i.e., the polycystic kidney disease model, termed ORPK mouse; Lehman et al., 2008) making studies using adult mice impossible, or they have severe problems with breeding or weaning. Moreover, the development of an experimentally induced loss of smell would more closely mirror the common human clinical conditions marked by acquired sensorineural anosmia or hyposmia, such as post-viral olfactory disorder or presbyosmia. We have developed a novel IH model based on producing ciliopathy selectively in OSNs regenerating after experimental lesion (Figure 2). We generated mice in which tamoxifen-inducible Cre-mediated excision of the intraflagellar transport protein IFT88 in the c-Kit lineage results in reconstitution of the OE with neurons lacking normal cilia, incapable of odor transduction. The c-Kit$^{CreERT2/+}$ driver has been extensively validated to drive efficient recombination in the OSN lineage (Goldstein et al., 2015; Goss et al., 2016).

Initially, IH mice were assessed 3 weeks after induction (Figures 2A–2C). Sections from control mice displayed a normal thick layer of neuronal cilia at the apical epithelial surface, visualized by labeling with antibody to acetylated tubulin. In contrast, the regenerated OE of tamoxifen-treated IH c-Kit$^{CreERT2/+}$; IFT88$^{fl/fl}$ mice lacked the thick layer of neuronal cilia (Figures 2B and 2C). The presence of minimal, patchy label is consistent with efficient recombination and generally ciliopathic OE. Electro-olfactogram (EOG) was used to test for olfactory neuron function (Figures 2D and 2E). Since the olfactory receptor proteins and accompanying odor transduction apparatus are localized to OSN cilia, EOG, which detects field responses at the OE surface, can measure olfactory loss due to ciliopathy (McIntyre et al., 2012). Electrophysiologic responses to amyl acetate, a widely used odorant that activates a broad range of olfactory receptors on OSNs, were diminished in IH mice compared with controls by >50%, comparing mean peak amplitudes (Figure 2E). The diminished, but not completely absent, olfactory sensitivity would be expected in an inducible model and resembles many acquired anosmic/hyposmic conditions in humans. Finally, we examined the degree of ongoing cilia depletion in a cohort of mice maintained for 10 weeks on the tamoxifen protocol. As expected from an inducible system, cilia loss was incomplete, yet remained significantly reduced compared with controls (Figure 2F). Overall, histologic and electrophysiologic assessments confirm that our IH mouse model provides a suitable host for testing of cell-based therapy for olfactory loss.

Cell-Treated Mice Recover Olfactory Function

We next asked whether the intranasal treatment of IH mice with wild-type eGFP-labeled c-KIT (+) GBCs would restore olfactory function. In initial experiments, IH mice received either cells (n = 4 mice) or vehicle (n = 5 mice); a control group received only methimazole, and neither tamoxifen nor cells, as a comparison for normal host OE reconstitution. Four weeks after engraftment, mice were euthanized for EOG testing of nasal tissue, as well as processing of tissue for histologic examination (Figure 3A).

Histologically, turbinate tissue was noted to contain large clusters of eGFP-labeled cells throughout the OE, morphologically consistent with engraftment-derived OSNs (Figures 3B–3F and S1). Quantification of engraftment-derived eGFP (+) cells revealed 368 ± 154 cells per coronal section, after applying Abercrombie correction (mean ± SEM, n = 4 host mice), reflecting robust engraftment overall. One mouse was found to have relatively poorer engraftment (Figure 3C) and was therefore excluded from further analyses. Tissue sections from engrafted mice were stained to detect cilia, using antibody to acetylated tubulin (Figures 3D and 3E). While patchy signal was identified across the OE of treated mice, there were clearly identifiable fields with robust cilia staining overlying eGFP (+) engraftment-derived neuronal somata and, at high magnification, their dendritic knobs (Figures 3D and 3E, box). Of interest,

Please cite this article in press as: Kurtenbach et al., Cell-Based Therapy Restores Olfactory Function in an Inducible Model of Hyposmia, Stem Cell Reports (2019), https://doi.org/10.1016/j.stemcr.2019.05.001

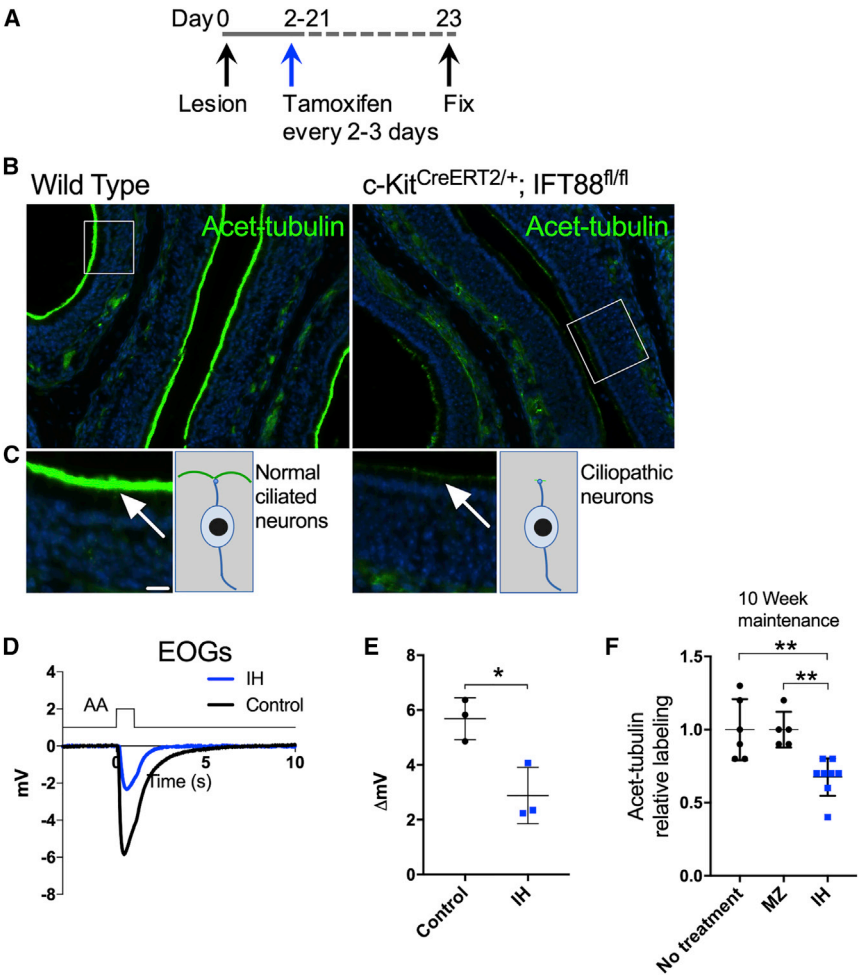

Figure 2. An Inducible Hyposmia (IH) Mouse Model Reconstitutes the OE with Non-functional Ciliopathic OSNs

(A) Experimental scheme is shown. During OE reconstitution induced by chemical lesion, tamoxifen delivery activates Cre-mediated deletion of the *Ift88* gene, required for cilia genesis, in the olfactory neuron lineage.

(B and C) (B) Tissue sections from representative wild-type control (left) or c-KitCre^{ERT2}; IFT88$^{fl/fl}$ (IH, right) mice demonstrate that the OE in IH mice lack the normal cilia layer at the apical surface, visualized with anti-acetylated tubulin staining (arrows, green) following drug treatment. Boxed areas are enlarged in (C). The cilia layer arises from the dendritic knobs of OSNs in normal OE.

(D) Electrophysiologic testing indicated that IH mice lack normal odor responses. Representative responses are shown; at least ten fields per subject were tested with a 0.1 M amyl acetate (AA) stimulus by air-phase electro-olfactogram (EOG) 3–4 weeks following IH drug regimen.

(E) Quantification of mean peak EOG responses per animal, mean ± SD (unpaired t test, two tailed, Welch's correction, n = 3 mice per group, *p = 0.02).

(F) Following 10 weeks of tamoxifen maintenance, acetylated tubulin labeling remained reduced in IH mice versus controls, mean ± SD (one-way ANOVA with multiple comparisons, n = 5–8 mice per group, **p = 0.004).

Scale bar: (C) 10 μm.

adjacent regions lacking eGFP (+) cells also lacked acetylated tubulin labeling, consistent with host OSNs in our IH mice remaining largely ciliopathic (Figure 3D, asterisk; see also Figure S2).

Labeled fibers were seen in the olfactory nerve and glomerular layer of the olfactory bulb (Figure 3F). Individual eGFP-labeled axon fibers could be seen terminating within most glomeruli; many of which were also found to harbor tyrosine hydroxylase (+) periglomerular cells (Figure 3F), indicative of odor-induced activity (Baker, 1990; Baker et al., 1983). Widespread glomerular innervation is consistent with engraftment-derived neurons expressing a full complement of olfactory receptors, which also function as guidance cues directing axons to appropriate glomeruli (Mombaerts et al., 1996).

EOG testing demonstrated improved odor responses in the cell-treated group (Figure 3G). As expected, there were many fields in cell-treated IH mice with minimal or small-amplitude responses, suggesting that these areas lacked engraftment-derived OSNs. However, testing also revealed areas in nasal specimens from cell-treated mice that yielded robust odor responses. These findings fit with an interpretation that there are scattered clusters of engraftment-derived odor-responsive neurons present across the nasal mucosa. Overall analysis comparing amyl acetate responses in vehicle-treated (−2.73 ± 1.4 mV, mean ± SD) and cell-treated (−4.03 ± 1.4mV) groups demonstrated improved EOG amplitudes following cellular therapy (p = 0.008).

Behavioral testing was also consistent with olfactory improvement in cell-treated mice. Experiments were repeated, preparing n = 10 mice in each group (controls, IH + vehicle, or IH + cell treatment) to permit behavior testing, since variability in mouse behavior assays are expected; 8–10 mice per group survived for analysis. Using a well-described odor behavior assay (Dewan et al., 2013), the time the mouse spent exploring a control versus an aversive odor was quantified (Figure 3H). Isopentylamine

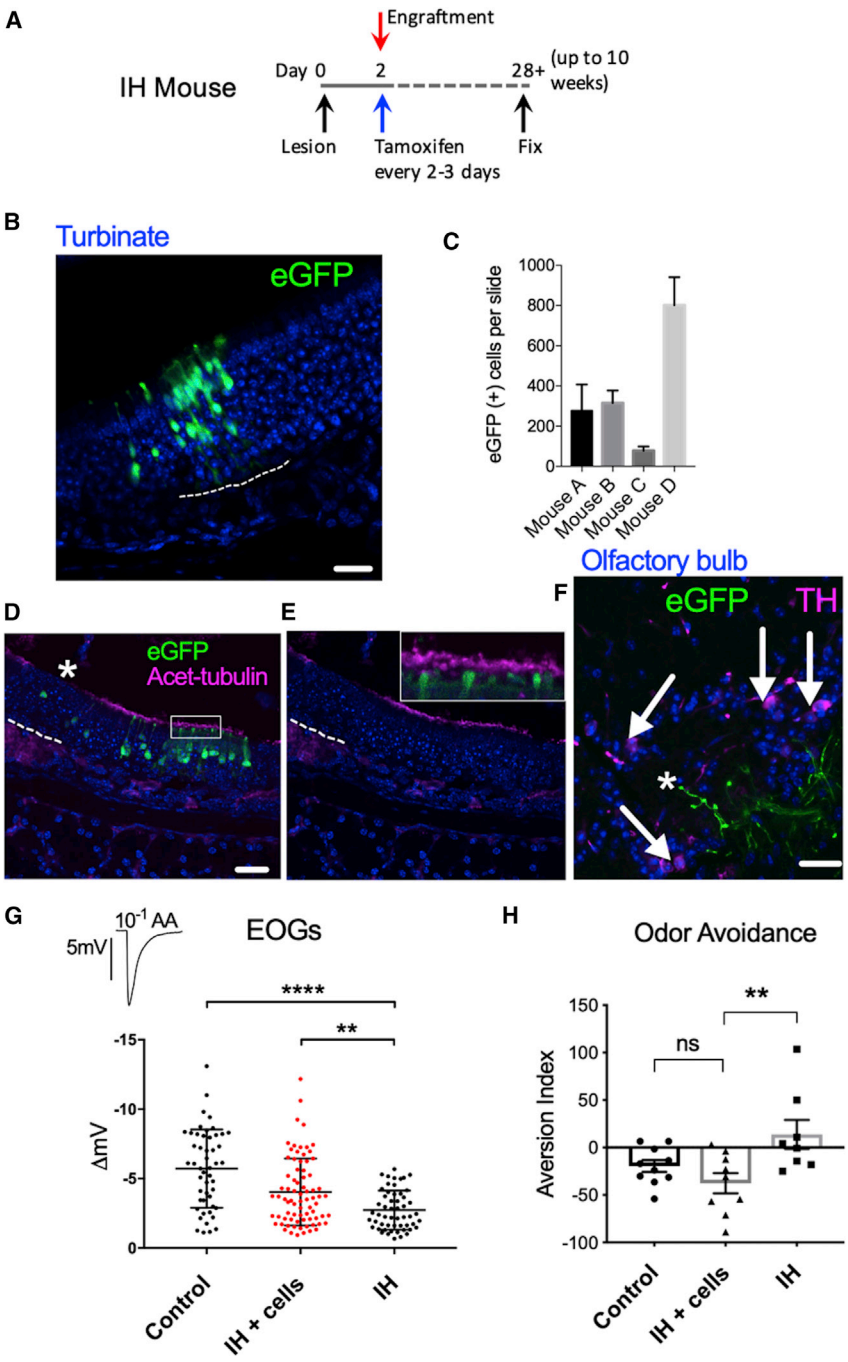

Figure 3. Basal Stem Cell Treatment of IH Mice Restores Olfaction

(A) Experimental paradigm is shown. The IH mouse model was used to test a cell-based therapy for the treatment of anosmia due to ciliopathy.

(B) Engraftment-derived eGFP-labeled cell clusters are distributed along the OE in tissue sections from treated mice; a typical cluster containing multiple eGFP-labeled olfactory neurons and microvillar or sustentacular cells is shown.

(C) Engrafted cells were quantified from histologic sections; columns represent mean Abercrombie-corrected total per slide, bar = SEM, n = 4 mice.

(D and E) Engraftment-derived cells are ciliated. Staining of OE for acetylated tubulin to label OSN cilia demonstrates cilia layer associated with dendritic knobs from eGFP (+) engraftment-derived cells (see boxed region). An adjacent eGFP (−) region lacks overlying cilia (asterisk).

(F) Engraftment-derived OSNs innervate the bulb. A single glomerulus is shown. On sections through the olfactory bulb, eGFP-labeled axons extending from engraftment-derived OSNs in the nose terminate (asterisk) within most glomeruli; arrows indicate tyrosine hydroxylase (+) periglomerular cells (magenta), typical of odor-induced glomerular activation.

(G) Electrophysiologic testing by EOG was performed on chemical-lesioned IH mice treated with vehicle (IH), cells (IH + cells), or controls that received no tamoxifen and therefore did not develop anosmia (Control); points on the graph indicate individual fields that were tested using amyl acetate 0.1 M (AA), n = 3–5 mice per group, mean ± SD shown. Increased EOG responses were found in cell-treated compared with vehicle-treated IH mice (**p = 0.0083, ANOVA with Kruskal-Wallis; ****p < 0.0001).

(H) Behavior assay provides additional evidence for restoration of olfactory input in cell-treated IH mice. Control and cell-treated mice demonstrate aversion to 10% isopentylamine (IPA) odor, while vehicle-treated IH mice do not. Aversion index = $time_{odor} - time_{water}$; **p = 0.008; ns = not significant; ANOVA, n = 8–10 mice, error bars = SEM.

Dashed line marks basal lamina in (B), (D), and (E). Scale bars: (B) 25 μm, (D and F) 20 μm.

(IPA), an aversive odorant detected only via olfactory neurons, was used for testing (Dewan et al., 2013; Green et al., 2018). Both the control group and the cell-treated group (IH + cells) displayed aversive responses to IPA, while the IH group did not (p = 0.008). These results are consistent with engraftment-derived olfactory neurons providing sufficient input to the olfactory bulbs to drive behavior.

Taken together, our results demonstrate evidence for engraftment, production of odor-responsive OSNs, reinnervation of the olfactory bulbs, and recovery of an

Please cite this article in press as: Kurtenbach et al., Cell-Based Therapy Restores Olfactory Function in an Inducible Model of Hyposmia, Stem Cell Reports (2019), https://doi.org/10.1016/j.stemcr.2019.05.001

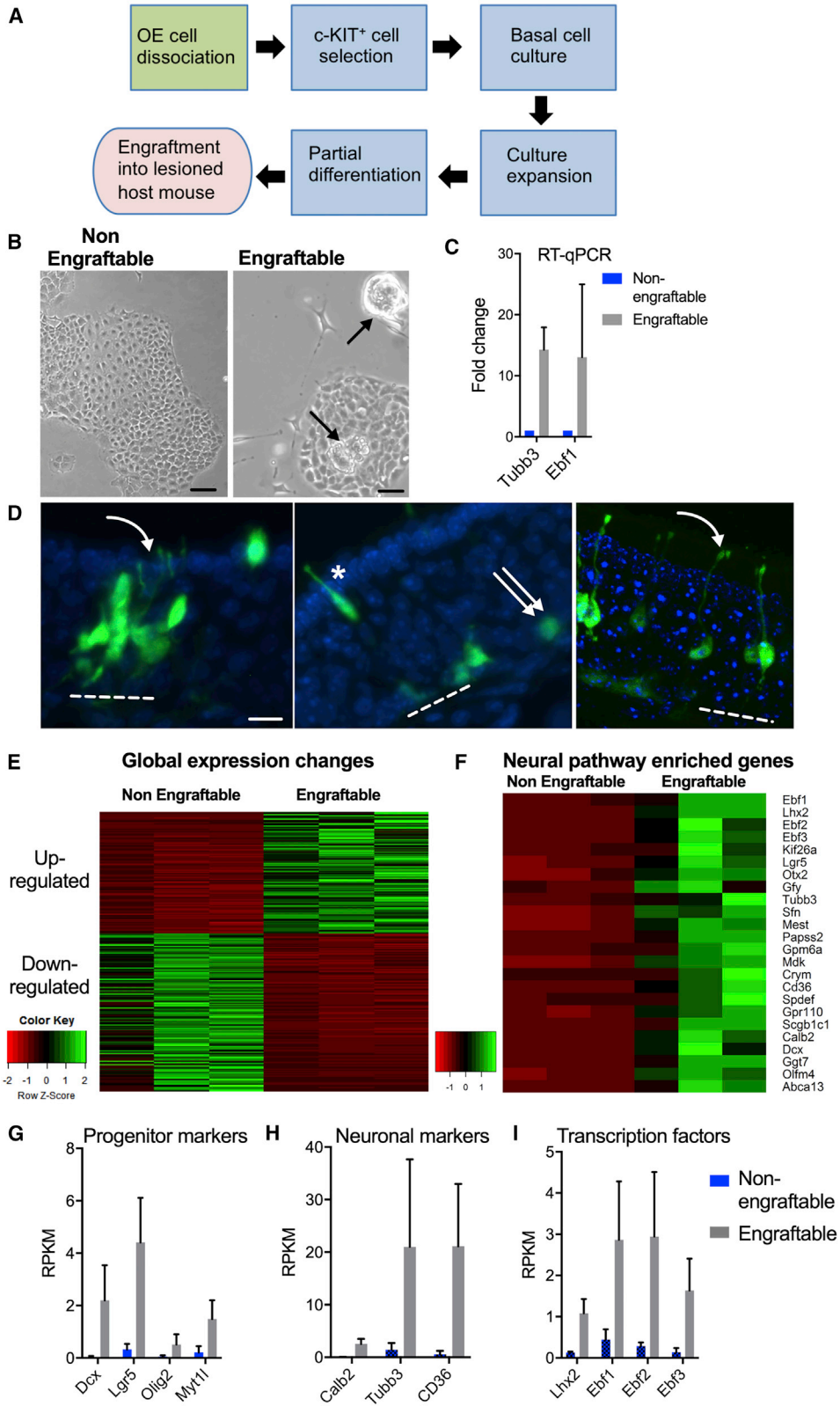

(legend on next page)

olfactory behavior in cell-treated mice. The efficiency of engraftment, producing several hundred OE cells per section, appears adequate to reestablish meaningful olfactory input in this model.

GBCs Expanded in Culture Remain Engraftment Competent

For potential translational use of adult GBCs, expansion of purified cells *in vitro* will be necessary. Therefore, we also tested the engraftment potential of cells that have been expanded in culture (Figure 4A). Previously, we described a culture model in which purified c-KIT (+) GBCs were capable of expansion in culture by inducing de-differentiation into SOX2 (+) adherent islands (Goldstein et al., 2016). Here, we have found that these de-differentiated cells do not engraft when infused intranasally (and refer to these cultures as "non-engraftable", Figure 4). Therefore, we modified the culture protocol to permit expansion and early differentiation, exposing cells for 12 h to RepSox, a specific inhibitor of the TGFβR1 receptor, rather than the continuous inhibitor exposure in our existing model. After 10 days, this culture condition yielded adherent islands, semi-adherent spheres, and process-bearing cellular outgrowth as the cultures expanded (Figure 4B). Comparing these modified cultures to our non-engraftable culture model, RT-qPCR demonstrated approximately a 10-fold increase in expression of olfactory neuron lineage genes Tubb3 and Ebf1 (n = 3 biological replicates, Figure 4C). Cultured GBCs prepared from eGFP-expressing mice using the modified protocol were tested by intranasal transplantation into wild-type hosts. As an assay for engraftment, following a 2-week recovery (Figure 4D), all mice were found to harbor engraftment-derived OE cells histologically. We found a low efficiency of engraftment with 11 ± 8.9 clusters per mouse (mean ± SD, n = 4 mice), nonetheless reflecting the presence of engraftment-competent cells in culture.

Molecular Characterization of Engraftment-Competent Cultures

We next sought to identify features that define engraftment competence *in vitro* and hypothesized that the transcriptional profile of these modified cultures should reflect lineage differentiation and the activation of relevant signaling pathways. We performed RNA sequencing (RNA-seq) on cells grown as engraftable cultures as well as cells grown in the standard de-differentiated culture model (non-engraftable) (Figure 4E). Using stringent analysis criteria, including a false discovery rate (FDR) <0.01, fold change of >2, and $p < 0.01$, approximately 800 genes were differentially expressed (Figure 4E). Considering the culture morphologies and the gene expression analysis, it is apparent that a mixture of cellular phenotypes emerge in the engraftable cultures. In accordance with these findings, Gene Ontology analysis (Table S2) for up- or downregulated genes included terms such as pluripotency signaling, cell differentiation, and nervous system development, as well as broader pathways such as differentiation, cell membrane, cell surface, and immune response. Nonetheless, focusing attention on upregulated genes in the neurogenic pathways enriched in the engraftable cultures (Figures 4F–4I), this subset includes neural progenitor markers such as *Dcx* (Duan et al., 2008; Jessberger et al., 2008), *Wnt* pathway/progenitor genes such as *Lgr5* (Chen et al., 2014), and olfactory neuron transcriptional regulators such as *Lhx2* and the *Ebf* family (Davis and Reed, 1996; Hirota and Mombaerts, 2004). Finally, olfactory sensory neuronal genes, including *Tubb3*, *Cd36*, and *Gfy*, are

Figure 4. Purified Olfactory Basal Cells Are Engraftable when Expanded *In Vitro* under Appropriate Culture Conditions and Display a Neurogenic Transcriptional Profile

(A) Experimental approach is shown schematically. The c-KIT (+) GBCs were purified from adult B6; eGFP (+) mice and tested for intranasal engraftment following expansion *in vitro* under modified culture conditions, as described.

(B) Phase-contrast images show morphology of non-engraftable (left) and modified engraftable cultures (right). Arrows mark semi-adherent sphere growth arising among expanding islands in engraftable cultures.

(C) Expression of neuronal lineage genes *Tubb3* and *Ebf1* was ≈10-fold increased compared with non-engraftable cultures by RT-qPCR (n = 3).

(D) GBCs expanded *in vitro* with the modified protocol were tested for intranasal engraftment. Representative histologic sections show engraftment-derived cell clusters in the OE; curved arrow indicates eGFP-labeled OSN dendrites. Engraftment-derived cells also remained as undifferentiated basal cells (double arrow, see also Figure S4) or produced microvillar sensory cells (asterisk). Dashed lines indicate basal lamina; n = 5 biological replicates.

(E) RNA-seq was performed on cultures maintained in standard conditions (non-engraftable) or modified conditions (engraftable). Heatmap shows 803 genes differentially expressed between the two culture conditions using stringent criteria, three biological replicates each, >2 fold change, FDR <0.01. Gene Ontology analysis is summarized in Table S2.

(F) Focused heatmap showing increased expression in engraftable cultures of several genes involved in olfactory neurogenesis.

(G–I) Expression of significantly increased progenitor cell markers (G), neuronal markers (H), or key transcription factors (I) involved in olfactory neurogenesis by RNA-seq.

Scale bars: (B) 30 μm (left) and 20 μm (right); (D) 10 μm.

Please cite this article in press as: Kurtenbach et al., Cell-Based Therapy Restores Olfactory Function in an Inducible Model of Hyposmia, Stem Cell Reports (2019), https://doi.org/10.1016/j.stemcr.2019.05.001

all highly enriched in the engraftable cultures (Kaneko-Goto et al., 2013; Lee et al., 2015; Xavier et al., 2016) (see also Figure S3 for culture immunocytochemistry). We conclude that purified c-KIT + cells cultured under appropriate conditions can give rise to a mixed population of renewing and differentiating cells, among which at least some cells are at an appropriate developmental stage for engraftment competence.

DISCUSSION

Cell-based therapy has potential for the treatment of olfactory sensory losses. Our results indicate that a purified murine adult olfactory stem cell treatment can rescue a mouse hyposmia model due to inducible ciliopathy. Treatment led to the development of engraftment-derived OSNs in the OE, the projection of their axons into the olfactory bulb of the brain, the development of improved electrophysiologic odor responses measured by EOG, and evidence for recovery at the behavioral level. Moreover, efforts to refine the culture conditions demonstrate that it is possible to promote the expansion of engraftment-competent purified adult GBCs.

A broad variety of clinical conditions are associated with hyposmia or anosmia, including genetic defects, trauma, aging, damage arising following viral upper respiratory infections, and conditions that are categorized as idiopathic. Available treatment options are lacking for all of these conditions. Whether the specific etiology causes OSN dysfunction, failures in maintenance of the OSN population, exhaustion within the basal cell neurogenic niche in the OE, or other poorly understood pathogenic etiologies, a cellular replacement therapy capable of restoring the OSN population holds promise for recovery of sensory function. Other therapeutic strategies, such as viral gene therapies, also hold potential for anosmia treatment, but these are usually tailored only to specific conditions, i.e., loss-of-function mutations (McIntyre et al., 2012). Accessing the OE at the olfactory cleft in humans requires only a simple, non-invasive nasal endoscopy, suggesting that the delivery of a local directed therapy is feasible. This accessibility contrasts with other sensory tissues, such as the cochlea, where delivery of a cell-based therapy has been reported in animal models of auditory neuropathy, but required meticulous invasive microsurgical access via the bony modiolus (Chen et al., 2012; Matsuoka et al., 2007).

Another consideration in a cell-based therapy for restoration of OSNs is the normal ongoing turnover within the OE. Would repeat treatments be necessary? The precise "normal" lifespan of specific OSNs is difficult to measure. OSNs are felt to live in the order of months (Carr and Farbman, 1993), but there is evidence for substantial variation, dependent on location within the nose in mice (Gaun et al., 2017). Also, there is clear evidence for activity-dependent mechanisms regulating OSN survival (Santoro and Dulac, 2012; Zhao and Reed, 2001). We found that, among the eGFP-labeled engraftment-derived cells identified here, some cells are localized among the basal cell layers (e.g., Figure 4D). This is expected, in that the c-KIT (+) population, used in the current treatment approach, has been demonstrated to produce mitotically quiescent or label-retaining GBCs via clonal-resolution genetic fate mapping using the Brainbow2.1 Cre-reporter (Goss et al., 2016). The behavior of subsets of GBCs as label retaining or reserve populations has been described in detail (Jang et al., 2014). We have also performed serial engraftment experiments, providing direct evidence for the serial repopulating potential of basal cells, a classic definition of stemness (Figure S4).

The ability of new OSNs arising from stem cell engraftment in the OE to connect their axons to the olfactory bulb of the brain is required to deliver sensory input. We find here that eGFP (+) axon fibers are abundant in the olfactory nerve and glomerular layers of the bulbs, suggesting robust innervation from engraftment-derived OSNs. Because of the lifelong turnover and replacement of OSNs under normal conditions, it is apparent that a permissive environment for axon growth and guidance exists in this tissue (Barnett and Riddell, 2004; Graziadei and Graziadei, 1979; Verhaagen et al., 1990). The normal recovery from severe chemical lesion has been well studied in rats and mice, documenting appropriate axon re-growth to the bulbs and generally accurate re-establishment of olfactory receptor topology in the bulbs (Cheung et al., 2013; Iwema et al., 2004). An important finding from recent studies testing viral gene therapy to rescue anosmic mice indicated that successful infection and rescue of only a small percentage of olfactory neurons was sufficient to deliver olfactory input, reflected in behavior testing (Green et al., 2018). Therefore, the necessary efficiency of either a cellular or viral therapy for olfactory loss appears to be easily achievable, at least in animal models.

Other translational challenges for stem cell therapies include potential safety concerns and identification of appropriate cell sources. Using a defined adult stem cell population, we found no evidence of tumor growth or migration of cells intracranially, at least in the time frame of this study. Production of appropriate human cells remains another challenge. However, the recent report of an ability to expand purified adult murine GBCs in culture (Goldstein et al., 2016) should inform efforts to manipulate and propagate similar populations from human OE. It is important to contrast the cell populations used here from reports that have utilized mesenchymal cell populations from human nasal tissue (Delorme et al., 2010; Murrell

et al., 2005; Nivet et al., 2011), highlighting the need for accurate nomenclature for adult "stem cells." To date, there is no evidence that the nasal mesenchymal cells are in the OSN lineage. Importantly, the c-KIT (+) GBCs used here arise in the OE, not the mesenchyme, and are bona fide OSN stem cells (Goldstein et al., 2015; Goss et al., 2016). Further attention directed at cultivating human GBCs *in vitro* is required; alternately, reprogramming efforts to direct other somatic cells toward an olfactory progenitor phenotype may be of interest. Analysis of our transcriptional profiling from engraftment-competent cultures may inform these efforts, providing insights into the cellular phenotypes that are most relevant, and features such as cell surface proteins that correlate with engraftment competence.

In summary, there is a need for development of novel therapies for correction of sensory losses (Bermingham-McDonogh et al., 2012). We report here evidence for the ability to utilize a cell-based therapy for the treatment of sensorineural olfactory loss in an adult animal model. These findings provide proof of principle for an approach that has the potential to be of broad utility for a range of clinical conditions causing anosmia.

EXPERIMENTAL PROCEDURES

Animals

The Institutional Animal Care and Use Committee, University of Miami, approved all procedures. Mice were bred on a C57BL/6 background. Mouse strains included wild-type C57BL/6J (Jackson Lab, Bar Harbor, ME), c-Kit$^{CreERT2/+}$ provided by Dr. Dieter Saur, Technical University of Munich (Klein et al., 2013), IFT88^{fl} (stock no. 022409, Jackson Laboratory) possessing loxP sites flanking exons 4–6 of the IFT88 gene (Haycraft et al., 2007), and B6-eGFP (stock no. 003291, Jackson Laboratory), which expresses eGFP strongly in widespread tissues. The IH mouse was generated by backcrossing to create the c-Kit$^{CreERT2/+}$; IFT88$^{fl/fl}$ genotype.

Methimazole lesion was induced by giving a single dose of 75 μg/g body weight intraperitoneally for IH mice or 50 μg/g for B6-eGFP mice. Tamoxifen (Sigma, St. Louis) was dissolved in peanut oil and delivered at 75 mg/kg daily for 5 days and continued every 2–3 days in adult mice to induce recombination, starting 1 day following methimazole administration.

Transplantation

B6-eGFP donor mice were lesioned with methimazole 8 days prior tissue collection. Cells from 3–4 mice were pooled for each host mouse engraftment. Host mice received methimazole 2 days prior to engraftment. Donor mice were decapitated following ketamine/xylazine anesthesia. Olfactory mucosa was collected from turbinates and septum, free of bone, and c-KIT (+) GBCs were purified based on immunomagnetic sorting, as described (Goldstein et al., 2016). Briefly, tissue was dissociated using collagenase 1 mg/mL, dispase 2 mg/mL with EDTA 1 mM for 20 min, followed by 2 min treatment with 0.0125% trypsin solution (Invitrogen). The reaction was stopped using fetal bovine serum (FBS), and cells were washed twice with Hank's balanced salt solution (HBSS) and passed through a 70 μm strainer. The pellet was resuspended in 300 μL of buffer (HBSS containing 2% FBS and 1 mM EDTA). Cells were incubated with APC-anti-c-KIT diluted 1:20 (eBioscience no. 17-1171, San Diego, CA; RRID: AB_469430) for 15 min, followed by APC magnetic selection kit (STEMCELL Technologies, Vancouver, Canada) per instructions. Cells were resuspended in a solution of DMEM:F12 with HEPES (Invitrogen, Carlsbad, CA) containing 5% basement membrane extract (Geltrex, Invitrogen no. A14132), 5% FBS (Invitrogen), penicillin-streptomycin (Invitrogen), n-acetylcysteine (5 μg/mL; Sigma), Y27632 10 μM (STEMCELL Technologies), and held on ice. Host mice were lightly anesthetized, and cells were introduced to the naris via 5–10 μL droplets in 5 min intervals, alternating between the nostrils. Approximately 25 μL total volume was delivered per naris.

Statistics

Statistical comparisons were performed with Prism 7 (GraphPad), using the appropriate t test or ANOVA. $p < 0.05$ is considered significant. When feasible, blinded analysis was performed. For histologic cell counts from adjacent 10 μm cryosections (Figure 3), cell soma of 6 μm was estimated and Abercrombie correction was applied $N = n \times (T/(T + d))$, where N = corrected count, n = cells counted per section, T = thickness of section, d = estimated cell soma diameter; each slide contained six adjacent sections, six slides per mouse. For EOG comparisons in Figure 3, testing indicated data were not normally distributed, therefore ANOVA with Kruskal-Wallis multiple comparison testing was used.

Cell Culture

To expand purified GBCs *in vitro*, we modified our previously detailed culture protocol (Goldstein et al., 2016) slightly. For "engraftable cultures," cells were selected based on c-KIT expression as described above and were plated onto gelatin-coated culture dishes at approximately 10^5 cells per well in NeuroCult NS-C Basal Medium, EGF 20 ng/mL, FGF2 10 ng/mL, heparin 2 μg/mL (all from STEMCELL Technologies), and penicillin-streptomycin (Invitrogen, Carlsbad, CA). RepSox (25 μM, STEMCELL Technologies), a TGF-β type 1 receptor (ALK5) inhibitor, was added along with Y27632 (10 μM, STEMCELL Technologies) overnight. Cultures were then maintained in base medium without inhibitors and were split 1:3 when 80% confluent, collecting both floating spheres and adherent cells. For "non-engraftable cultures," additional cultures were prepared following our published protocol exactly, maintained in NS-C medium with SB431542 (10 μM) and BMP4 (10 ng/mL). For both culture preparations, >3 biological replicates were prepared using cells pooled from three mouse noses for each sample.

Electro-olfactograms

Air-phase EOGs were performed following established protocols (Cygnar et al., 2010). Details and reagents are provided in Supplemental Information.

Behavioral Assays

An olfactory avoidance assay was modified from published protocols (Dewan et al., 2013). Testing took place during the nocturnal phase. Freshly cleaned standard mouse housing cages without bedding were used as test arenas, divided into an odorized compartment with a curtain, covered with a plexiglass lid. Testing was performed in dim red light conditions, blocking visual cues or distractions. Mice were recorded using an infrared camera. The mice were habituated in the test arena for 3 min. Whatman 1 filter paper circles (2.5 cm diameter) in a 35 mm Petri dish were either impregnated with 20 μL of water as odorless control or with 10% IPA to test the ability to detect an aversive scent. The time spent investigating the odorized chamber was analyzed. Aversion index = $time_{odor} - time_{water}$. Control, IH mice, and cell-treated IH mice were tested 8–10 weeks post treatment (n = 8–10 mice per group), and data were analyzed by ANOVA with multiple comparisons.

RNA Sequencing

RNA-Seq Sample Preparation

Total RNA was prepared from olfactory cultures using column purification per protocol (Zymo Research Corp., Irvine, CA, USA). DNase I on-column digestion was performed. Samples were prepared in biological triplicates. Preparation and sequencing of RNA libraries was carried out in the John P. Hussman Institute for Human Genomics Center for Genome Technology (University of Miami Miller School of Medicine). Quality analysis was performed using an Agilent Bioanalyzer to confirm RNA integrity score >9. Using 500 ng of total RNA as input, the TruSeq Stranded Total RNA Library Prep Kit with Ribo-Zero (Illumina, San Diego, CA) was used to create ribosomal RNA-depleted sequencing libraries. Each sample had a unique barcode to allow for multiplexing and was sequencing to 35 million raw reads in a single-end 75 bp sequencing run on the Illumina NextSeq500.

RNA-Seq Bioinformatics Analysis

Raw sequence data were processed by the on-instrument Real Time Analysis software (v.2.4.11) to basecall files that were converted to de-multiplexed FASTQ files with the Illumina supplied scripts in the BCL2FASTQ software (v2.17). The quality of the reads was determined with FASTQC software (http://www.bioinformatics.babraham.ac.uk/projects/fastqc/) for per base sequence quality, duplication rates, and overrepresented k-mers. Illumina adapters were trimmed from the ends of the reads using the Trim Galore! package (http://www.bioinformatics.babraham.ac.uk/projects/trim_galore/). Reads were aligned to the mouse reference genome (mm10) with the STAR aligner (v2.5.0a) (Dobin et al., 2013). Gene count quantification for total RNA was performed using the GeneCounts function within STAR against the ENSEMBL v77 mouse transcript.gtf file.

Differential Expression and Pathway Analysis

Gene count data were input into edgeR software (Robinson et al., 2010) for differential expression analysis. Briefly, gene counts were normalized using the trimmed mean of M values (TMM) (Robinson and Oshlack, 2010) method to account for compositional difference between the libraries. Group differential expression was calculated using the generalized linear model likelihood ratio test (glmLRT) function implemented in edgeR. Genes meeting a nominally significant threshold ($p < 0.05$ and fold change ±1.5) were input into The Database for Annotation, Visualization and Integrated Discovery (DAVID) v6.8 for pathway enrichment analysis (Huang da et al., 2009a, 2009b).

Immunochemistry and RT-qPCR

Details and reagents are provided in Supplemental Information.

ACCESSION NUMBERS

Sequence data generated from the RNA-sequencing experiments have been deposited in GEO under accession number GEO: GSE124443.

SUPPLEMENTAL INFORMATION

Supplemental Information can be found online at https://doi.org/10.1016/j.stemcr.2019.05.001.

AUTHOR CONTRIBUTIONS

B.J.G., N.C., J.M.H., and S.K. designed the research; S.K., G.M.G., S.G., R.C., and B.J.G. performed experiments; S.K., G.M.G., S.G., N.C., R.C., and B.J.G. analyzed data; S.K. and B.J.G. wrote the manuscript; N.C., J.M.H., and B.J.G. edited the paper.

DECLARATION OF INTERESTS

J.M.H. discloses a financial interest with Longeveron.

ACKNOWLEDGMENTS

This work was funded by National Institutes of Health grants DC013556 and DC016859 (B.J.G.) and a Clinician-Scientist Award from the American College of Surgeons/Triological Society (B.J.G.). We thank Dr. Anthony Griswold for expert assistance with RNA-seq analysis and Dr. Dieter Saur for providing c-Kit Cre-expressing mice.

Received: September 10, 2018
Revised: April 30, 2019
Accepted: May 2, 2019
Published: May 30, 2019

REFERENCES

Baker, H. (1990). Unilateral, neonatal olfactory deprivation alters tyrosine hydroxylase expression but not aromatic amino acid decarboxylase or GABA immunoreactivity. Neuroscience *36*, 761–771.

Baker, H., Kawano, T., Margolis, F.L., and Joh, T.H. (1983). Transneuronal regulation of tyrosine hydroxylase expression in olfactory bulb of mouse and rat. J. Neurosci. *3*, 69–78.

Barnett, S.C., and Riddell, J.S. (2004). Olfactory ensheathing cells (OECs) and the treatment of CNS injury: advantages and possible caveats. J. Anat. *204*, 57–67.

Bergman, U., Ostergren, A., Gustafson, A.L., and Brittebo, B. (2002). Differential effects of olfactory toxicants on olfactory regeneration. Arch. Toxicol. *76*, 104–112.

Bermingham-McDonogh, O., Corwin, J.T., Hauswirth, W.W., Heller, S., Reed, R., and Reh, T.A. (2012). Regenerative medicine for the special senses: restoring the inputs. J. Neurosci. *32*, 14053–14057.

Brunet, L.J., Gold, G.H., and Ngai, J. (1996). General anosmia caused by a targeted disruption of the mouse olfactory cyclic nucleotide-gated cation channel. Neuron *17*, 681–693.

Buck, L., and Axel, R. (1991). A novel multigene family may encode odorant receptors: a molecular basis for odor recognition. Cell *65*, 175–187.

Calof, A.L., Bonnin, A., Crocker, C., Kawauchi, S., Murray, R.C., Shou, J., and Wu, H.H. (2002). Progenitor cells of the olfactory receptor neuron lineage. Microsc. Res. Tech. *58*, 176–188.

Carr, V.M., and Farbman, A.I. (1993). The dynamics of cell death in the olfactory epithelium. Exp. Neurol. *124*, 308–314.

Chen, M., Tian, S., Yang, X., Lane, A.P., Reed, R.R., and Liu, H. (2014). Wnt-responsive Lgr5(+) globose basal cells function as multipotent olfactory epithelium progenitor cells. J. Neurosci. *34*, 8268–8276.

Chen, W., Jongkamonwiwat, N., Abbas, L., Eshtan, S.J., Johnson, S.L., Kuhn, S., Milo, M., Thurlow, J.K., Andrews, P.W., Marcotti, W., et al. (2012). Restoration of auditory evoked responses by human ES-cell-derived otic progenitors. Nature *490*, 278–282.

Chen, X., Fang, H., and Schwob, J.E. (2004). Multipotency of purified, transplanted globose basal cells in olfactory epithelium. J. Comp. Neurol. *469*, 457–474.

Cheung, M.C., Jang, W., Schwob, J.E., and Wachowiak, M. (2013). Functional recovery of odor representations in regenerated sensory inputs to the olfactory bulb. Front. Neural Circuits *7*, 207.

Cygnar, K.D., Stephan, A.B., and Zhao, H. (2010). Analyzing responses of mouse olfactory sensory neurons using the air-phase electroolfactogram recording. J. Vis. Exp. https://doi.org/10.3791/1850.

Davis, J.A., and Reed, R.R. (1996). Role of Olf-1 and Pax-6 transcription factors in neurodevelopment. J. Neurosci. *16*, 5082–5094.

Delorme, B., Nivet, E., Gaillard, J., Haupl, T., Ringe, J., Deveze, A., Magnan, J., Sohier, J., Khrestchatisky, M., Roman, F.S., et al. (2010). The human nose harbors a niche of olfactory ectomesenchymal stem cells displaying neurogenic and osteogenic properties. Stem Cells Dev. *19*, 853–866.

Dewan, A., Pacifico, R., Zhan, R., Rinberg, D., and Bozza, T. (2013). Non-redundant coding of aversive odours in the main olfactory pathway. Nature *497*, 486–489.

Dobin, A., Davis, C.A., Schlesinger, F., Drenkow, J., Zaleski, C., Jha, S., Batut, P., Chaisson, M., and Gingeras, T.R. (2013). STAR: ultrafast universal RNA-seq aligner. Bioinformatics *29*, 15–21.

Doty, R.L., Shaman, P., Applebaum, S.L., Giberson, R., Siksorski, L., and Rosenberg, L. (1984). Smell identification ability: changes with age. Science *226*, 1441–1443.

Duan, X., Kang, E., Liu, C.Y., Ming, G.L., and Song, H. (2008). Development of neural stem cell in the adult brain. Curr. Opin. Neurobiol. *18*, 108–115.

Fletcher, R.B., Das, D., Gadye, L., Street, K.N., Baudhuin, A., Wagner, A., Cole, M.B., Flores, Q., Choi, Y.G., Yosef, N., et al. (2017). Deconstructing olfactory stem cell trajectories at single-cell resolution. Cell Stem Cell *20*, 817–830.e8.

Fletcher, R.B., Prasol, M.S., Estrada, J., Baudhuin, A., Vranizan, K., Choi, Y.G., and Ngai, J. (2011). p63 regulates olfactory stem cell self-renewal and differentiation. Neuron *72*, 748–759.

Gaun, V., Zunitch, M.J., Lin, B., Jang, W. and Schwob, J.E. (2017). The lifespan of olfactory sensory neurons. Association for Chemoreception Sciences 39th Annual Meeting.

Goldstein, B.J., Fang, H., Youngentob, S.L., and Schwob, J.E. (1998). Transplantation of multipotent progenitors from the adult olfactory epithelium. Neuroreport *9*, 1611–1617.

Goldstein, B.J., Goss, G.M., Choi, R., Saur, D., Seidler, B., Hare, J.M., and Chaudhari, N. (2016). Contribution of Polycomb group proteins to olfactory basal stem cell self-renewal in a novel c-KIT+ culture model and in vivo. Development *143*, 4394–4404.

Goldstein, B.J., Goss, G.M., Hatzistergos, K.E., Rangel, E.B., Seidler, B., Saur, D., and Hare, J.M. (2015). Adult c-Kit(+) progenitor cells are necessary for maintenance and regeneration of olfactory neurons. J. Comp. Neurol. *523*, 15–31.

Goss, G.M., Chaudhari, N., Hare, J.M., Nwojo, R., Seidler, B., Saur, D., and Goldstein, B.J. (2016). Differentiation potential of individual olfactory c-Kit+ progenitors determined via multicolor lineage tracing. Dev. Neurobiol. *76*, 241–251.

Graziadei, G.A., and Graziadei, P.P. (1979). Neurogenesis and neuron regeneration in the olfactory system of mammals. II. Degeneration and reconstitution of the olfactory sensory neurons after axotomy. J. Neurocytol. *8*, 197–213.

Green, W.W., Uytingco, C.R., Ukhanov, K., Kolb, Z., Moretta, J., McIntyre, J.C., and Martens, J.R. (2018). Peripheral gene therapeutic rescue of an olfactory ciliopathy restores sensory input, axonal pathfinding, and odor-guided behavior. J. Neurosci. *38*, 7462–7475.

Guillemot, F., Lo, L.C., Johnson, J.E., Auerbach, A., Anderson, D.J., and Joyner, A.L. (1993). Mammalian achaete-scute homolog 1 is required for the early development of olfactory and autonomic neurons. Cell *75*, 463–476.

Haycraft, C.J., Zhang, Q., Song, B., Jackson, W.S., Detloff, P.J., Serra, R., and Yoder, B.K. (2007). Intraflagellar transport is essential for endochondral bone formation. Development *134*, 307–316.

Hirota, J., and Mombaerts, P. (2004). The LIM-homeodomain protein Lhx2 is required for complete development of mouse olfactory sensory neurons. Proc. Natl. Acad. Sci. U S A *101*, 8751–8755.

Hoffman, H.J., Rawal, S., Li, C.M., and Duffy, V.B. (2016). New chemosensory component in the U.S. National Health and Nutrition Examination Survey (NHANES): first-year results for measured olfactory dysfunction. Rev. Endocr. Metab. Disord. *17*, 221–240.

Holbrook, E.H., Leopold, D.A., and Schwob, J.E. (2005). Abnormalities of axon growth in human olfactory mucosa. Laryngoscope *115*, 2144–2154.

Huang da, W., Sherman, B.T., and Lempicki, R.A. (2009a). Bioinformatics enrichment tools: paths toward the comprehensive functional analysis of large gene lists. Nucleic Acids Res. *37*, 1–13.

Huang da, W., Sherman, B.T., and Lempicki, R.A. (2009b). Systematic and integrative analysis of large gene lists using DAVID bioinformatics resources. Nat. Protoc. *4*, 44–57.

Huard, J.M., Youngentob, S.L., Goldstein, B.J., Luskin, M.B., and Schwob, J.E. (1998). Adult olfactory epithelium contains multipotent progenitors that give rise to neurons and non-neural cells. J. Comp. Neurol. *400*, 469–486.

Iwema, C.L., Fang, H., Kurtz, D.B., Youngentob, S.L., and Schwob, J.E. (2004). Odorant receptor expression patterns are restored in lesion-recovered rat olfactory epithelium. J. Neurosci. *24*, 356–369.

Jang, W., Chen, X., Flis, D., Harris, M., and Schwob, J.E. (2014). Label-retaining, quiescent globose basal cells are found in the olfactory epithelium. J. Comp. Neurol. *522*, 731–749.

Jang, W., Lambropoulos, J., Woo, J.K., Peluso, C.E., and Schwob, J.E. (2008). Maintaining epitheliopoietic potency when culturing olfactory progenitors. Exp. Neurol. *214*, 25–36.

Jessberger, S., Toni, N., Clemenson, G.D., Jr., Ray, J., and Gage, F.H. (2008). Directed differentiation of hippocampal stem/progenitor cells in the adult brain. Nat. Neurosci. *11*, 888–893.

Kaneko-Goto, T., Sato, Y., Katada, S., Kinameri, E., Yoshihara, S., Nishiyori, A., Kimura, M., Fujita, H., Touhara, K., Reed, R.R., et al. (2013). Goofy coordinates the acuity of olfactory signaling. J. Neurosci. *33*, 12987–12996.

Kern, R.C., Quinn, B., Rosseau, G., and Farbman, A.I. (2000). Post-traumatic olfactory dysfunction. Laryngoscope *110*, 2106–2109.

Klein, S., Seidler, B., Kettenberger, A., Sibaev, A., Rohn, M., Feil, R., Allescher, H.D., Vanderwinden, J.M., Hofmann, F., Schemann, M., et al. (2013). Interstitial cells of Cajal integrate excitatory and inhibitory neurotransmission with intestinal slow-wave activity. Nat. Commun. *4*, 1630.

Lee, S., Eguchi, A., Tsuzuki, S., Matsumura, S., Inoue, K., Iwanaga, T., Masuda, D., Yamashita, S., and Fushiki, T. (2015). Expression of CD36 by olfactory receptor cells and its abundance on the epithelial surface in mice. PLoS One *10*, e0133412.

Lehman, J.M., Michaud, E.J., Schoeb, T.R., Aydin-Son, Y., Miller, M., and Yoder, B.K. (2008). The Oak Ridge Polycystic Kidney mouse: modeling ciliopathies of mice and men. Dev. Dyn. *237*, 1960–1971.

Leung, C.T., Coulombe, P.A., and Reed, R.R. (2007). Contribution of olfactory neural stem cells to tissue maintenance and regeneration. Nat. Neurosci. *10*, 720–726.

Matsuoka, A.J., Kondo, T., Miyamoto, R.T., and Hashino, E. (2007). Enhanced survival of bone-marrow-derived pluripotent stem cells in an animal model of auditory neuropathy. Laryngoscope *117*, 1629–1635.

McIntyre, J.C., Davis, E.E., Joiner, A., Williams, C.L., Tsai, I.C., Jenkins, P.M., McEwen, D.P., Zhang, L., Escobado, J., Thomas, S., et al. (2012). Gene therapy rescues cilia defects and restores olfactory function in a mammalian ciliopathy model. Nat. Med. *18*, 1423–1428.

Mombaerts, P., Wang, F., Dulac, C., Chao, S.K., Nemes, A., Mendelsohn, M., Edmondson, J., and Axel, R. (1996). Visualizing an olfactory sensory map. Cell *87*, 675–686.

Murphy, C., Schubert, C.R., Cruickshanks, K.J., Klein, B.E., Klein, R., and Nondahl, D.M. (2002). Prevalence of olfactory impairment in older adults. JAMA *288*, 2307–2312.

Murrell, W., Feron, F., Wetzig, A., Cameron, N., Splatt, K., Bellette, B., Bianco, J., Perry, C., Lee, G., and Mackay-Sim, A. (2005). Multipotent stem cells from adult olfactory mucosa. Dev. Dyn. *233*, 496–515.

Nivet, E., Vignes, M., Girard, S.D., Pierrisnard, C., Baril, N., Deveze, A., Magnan, J., Lante, F., Khrestchatisky, M., Feron, F., et al. (2011). Engraftment of human nasal olfactory stem cells restores neuroplasticity in mice with hippocampal lesions. J. Clin. Invest. *121*, 2808–2820.

Paik, S.I., Lehman, M.N., Seiden, A.M., Duncan, H.J., and Smith, D.V. (1992). Human olfactory biopsy. The influence of age and receptor distribution. Arch. Otolaryngol. Head Neck Surg. *118*, 731–738.

Robinson, M.D., McCarthy, D.J., and Smyth, G.K. (2010). edgeR: a Bioconductor package for differential expression analysis of digital gene expression data. Bioinformatics *26*, 139–140.

Robinson, M.D., and Oshlack, A. (2010). A scaling normalization method for differential expression analysis of RNA-seq data. Genome Biol. *11*, R25.

Santoro, S.W., and Dulac, C. (2012). The activity-dependent histone variant H2BE modulates the life span of olfactory neurons. Elife *1*, e00070.

Schwob, J.E., Jang, W., Holbrook, E.H., Lin, B., Herrick, D.B., Peterson, J.N., and Hewitt Coleman, J. (2017). Stem and progenitor cells of the mammalian olfactory epithelium: taking poietic license. J. Comp. Neurol. *525*, 1034–1054.

Seiden, A.M. (2004). Postviral olfactory loss. Otolaryngol. Clin. North Am. *37*, 1159–1166.

Tietjen, I., Rihel, J.M., Cao, Y., Koentges, G., Zakhary, L., and Dulac, C. (2003). Single-cell transcriptional analysis of neuronal progenitors. Neuron *38*, 161–175.

Verhaagen, J., Greer, C.A., and Margolis, F.L. (1990). B-50/GAP43 gene expression in the rat olfactory system during postnatal development and aging. Eur. J. Neurosci. *2*, 397–407.

Williams, C.L., McIntyre, J.C., Norris, S.R., Jenkins, P.M., Zhang, L., Pei, Q., Verhey, K., and Martens, J.R. (2014). Direct evidence for BBSome-associated intraflagellar transport reveals distinct properties of native mammalian cilia. Nat. Commun. *5*, 5813.

Wrobel, B.B., and Leopold, D.A. (2004). Clinical assessment of patients with smell and taste disorders. Otolaryngol. Clin. North Am. *37*, 1127–1142.

Xavier, A.M., Ludwig, R.G., Nagai, M.H., de Almeida, T.J., Watanabe, H.M., Hirata, M.Y., Rosenstock, T.R., Papes, F., Malnic, B., and Glezer, I. (2016). CD36 is expressed in a defined subpopulation of neurons in the olfactory epithelium. Sci. Rep. *6*, 25507.

Zhao, H., and Reed, R.R. (2001). X inactivation of the OCNC1 channel gene reveals a role for activity-dependent competition in the olfactory system. Cell *104*, 651–660.

Stem Cell Reports, Volume *12*

Supplemental Information

Cell-Based Therapy Restores Olfactory Function in an Inducible Model of Hyposmia

Sarah Kurtenbach, Garrett M. Goss, Stefania Goncalves, Rhea Choi, Joshua M. Hare, Nirupa Chaudhari, and Bradley J. Goldstein

Supplemental Information

SI Materials and Methods

Tissue processing and staining

Adult mice were euthanized under ketamine–xylazine anesthesia by exsanguination by perfusion with PBS followed by 4% paraformaldehyde in phosphate buffer. Nasal tissue was dissected and postfixed for 2 hours, rinsed in PBS, and then cryoprotected with 30% sucrose/250 mM EDTA in PBS for 3-5 days. Specimens were then embedded in O.C.T. compound (VWR, Radnor, PA) frozen in liquid nitrogen and cryosectioned at 10 μm. Cultures were fixed 15-30 minutes and rinsed in PBS. Primary antibodies diluted into 5% normal serum, 0.01% Triton x-100, 5% nonfat milk, and phosphate buffered saline were incubated overnight at 4 °C. Alexa-594 conjugated secondary antibodies (Jackson ImmunoResearch) were applied 45 min at room temperature, followed by DAPI nuclear staining. For anti-c-KIT staining, heat mediated antigen retrieval in sodium citrate was performed.

Primary antibodies included: rabbit anti-c-Kit, 1:30 (Cell Signaling Technology #3074, RRID: AB_10829442); mouse anti-acetylated tubulin, 1:1000 (Sigma, #T6793, RRID: AB_477585); mouse anti-tyrosine hydroxylase, 1:500 (Millipore #MAB318, RRID: AB_ 2201528); mouse Tuj1 against neuron-specific β-tubulin (Biolegend MMS-435P-250, RRID: AB_2313773); rabbit anti-CK18 (Abcam #ab32118, RRID: AB_736394); rabbit anti-Trpm5 (Alamone labs Jerusalem, Israel, #ACC-045, RRID: AB_2040252); rabbit anti-GAP43 (Abcam #ab75810, Cambridge, MA, RRID: AB_1310252); rabbit anti-CD36 (Cell Signaling

Technology #14347); rat anti-SOX2 (eBioscience 14-9811-82. RRID: AB_11219471). All antibodies were extensively validated by knockout or multiple other approaches, as recommended(Uhlen et al., 2016). Visualization of eGFP in tissue sections did not require anti-GFP staining.

Staining was analyzed on an Olympus IX81 epifluorescent microscope or a Zeiss LSM-710 confocal microscope. Pseudocoloration and brightness/contrast adjustment were performed using ImageJ. Parallel settings for capture and adjustment were used for images included in the same figure. For phase contrast cell culture microscopy, brightness/contrast were adjusted in ImageJ.

An estimate of cilia loss was quantified from acetylated-tubulin stained tissue sections (n=5-8 mice per group) using ImageJ. We stained tissue from mice maintained on tamoxifen for 10 weeks, versus controls, to determine how much recovery might occur from cells that did not undergo Cre-mediated recombination. Images were acquired using identical microscope and camera settings using Leica software and a Leica DMi8 instrument. In ImageJ, a saved region-of-interest template was used to outline the cilia layer in images along turbinates II, III and corresponding nasal septum from control, MZ-only, or MZ and tamoxifen-treated (IH) mice. The average pixel intensity was obtained from ImageJ measurement tools. All staining was done in parallel using the same primary and secondary antibody dilution preparations. However, background levels still vary slightly among sections, so several ROIs from the airspace and non-cilia region within the OE were also measured and averaged to subtract each mean background level from each section. Mean and s.d. for each group was then analyzed in Prism (ANOVA), normalizing the background-corrected measures against the MZ-only (ciliated) controls.

RT-qPCR

Total RNA was isolated using column purification per protocol (Zymo Research Corp., Irvine, CA, USA). DNase I on-column digestion was performed. Reverse transcription first strand cDNA synthesis was performed using Superscript IV (Invitrogen). Taqman assays (Invitrogen) were used in reactions performed on a BioRad real time thermal cycler (**Supplemental Table 1)**. Reactions were performed in triplicate and at least 3 biologic replicates were tested per condition. Fold-change calculations were performed using the $2^{-\Delta\Delta Ct}$ technique(Livak and Schmittgen, 2001), and GAPDH or RPO expression was used as a reference.

Supplementary Table 1. PCR reagents.

Gene	Gene Name	Assay ID (Applied Biosystems)
Neurog1	Neurogenin 1	Mm00440466_s1
Tubb3	Tubulin, beta 3 class III	Mm00727586_s1
Gapdh	Glyceraldehyde-3-phosphate dehydrogenase	Mm99999915_g1

Table S1. Assays used for RT-qPCRs are listed. All Taqman probes were obtained from Applied Biosystems (Thermo Fisher, Waltham MA, USA).

Electro-olfactograms. Briefly, septum or medial turbinate tissue was placed in Ringer's solution with a reference electrode. A recording electrode with a 5-10μm diameter was

prepared and advanced via micromanipulator to contact the mucosal surface (cilia) under a dissecting microscope, producing a flat line on oscilloscope trace. Continuous humidified air was applied over the tissue. Odor stimulus was introduced into the stream for 0.1-1 sec pulse using a picospritzer (Parker Hannifin). Depolarization responses were recorded and digitized for analysis (Axograph software). An amplifier (Warner DP-301) in DC mode with 100x gain and a low-pass filter was used, connected to a digitizer (Digidata 1500, Axon Instruments), with output connected to a laptop computer triggering picospritzer. EOGs are displayed as mV depolarizations / time. Odors with broad stimulus activity such as amyl acetate were used, prepared fresh prior to procedure as stocks in DMSO, further diluted 50-fold into water in vials to equilibrate into vapor phase. Vials were attached via a port into the humidified airstream. The apparatus is housed in a Faraday cage. We recorded from ≈10 stereotyped areas from septum and turbinates II or III from controls and experimental mice. Mean ± s.d. peak amplitudes from at least 10 fields using the same stimulus (i.e. 10^{-1}M amyl acetate) were compared statistically from control, IH, and cell-treated IH mice, using ANOVA with Kruskal-Wallis testing.

SI Figures

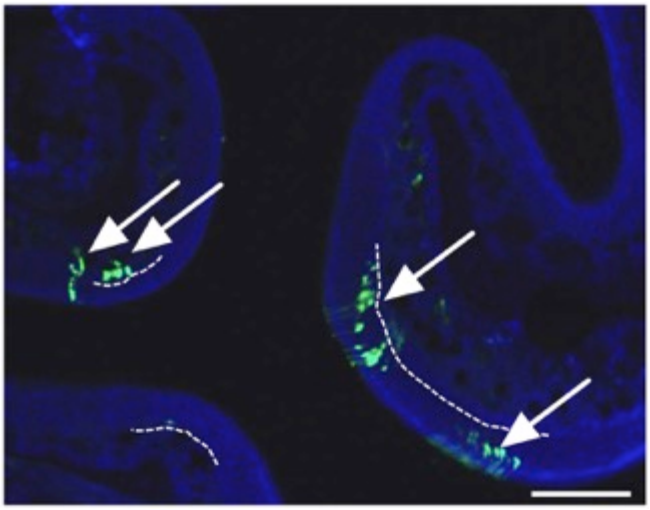

Figure S1. At low magnification, widespread engraftment is evident. eGFP+ engraftment-derived clusters (green) in the olfactory mucosa are present on multiple turbinates (arrows). Double arrow indicates a cluster containing Bowman's gland cells in the lamina propria, below the basement membrane of the OE (dashed lines). The other clusters contain OSNs, with dendrites visible extending apically to the nasal airspace. The density of engraftment in this field is typical of the results identified here. Nuclei are counterstained with DAPI (blue). Bar 100 μm.

Supplementary Table 2. Gene Ontology analysis.

GO of targets upregulated in engraftable cultures	Enrichment	Benjamini
GO:0045087 innate immune response	3.26	0.013
GO:0030154 cell differentiation	2.52	0.030
GO:0009986 cell surface	2.22	0.042
GO:0005615 extracellular space	2.16	4.16E-05
GO:0005576 extracellular region	2.07	5.42E-05
GO:0070062 extracellular exosome	1.74	1.82E-04
GO:0016020 membrane	1.34	7.77E-04
GO:0005886 plasma membrane	1.3	0.030
GO of targets downregulated in engraftable cultures	Enrichment	Benjamini
GO:0042476 odontogenesis	16.1	0.007
GO:0007417central nervous system development	6.98	0.012
GO:0050679 positive regulation of epithelial cell proliferation	6.54	0.049
GO:0005604 basement membrane	6.49	0.003
mmu04115 p53 signaling pathway	6.35	0.035
mmu04550 Signaling pathways regulating pluripotency of stem cells	4.85	0.015
GO:0031012 extracellular matrix	3.00	0.038

Table S2. Gene Ontology analysis for RNA-seq performed on engraftment-competent olfactory basal cell cultures versus non-engraftable de-differentiated olfactory basal cell cultures. Engraftable cultures were prepared from purified c-KIT+ basal cells exposed overnight to RepSox (25 μM) and then maintained in NS-C medium (Stemcell Tech); non-engraftable cultures were identical except that they were maintained in NS-C with SB431542 (10 μM) and BMP4 (10 ng/ml)(Goldstein et al., 2016). Selected top GO or KEGG pathway terms that are induced (top) or repressed (bottom) in engraftable cultures are listed here, determined in DAVID. For each term, enrichment scores and Benjamini values are listed. In the induced clusters, the terms “cell differentiation” and “cell surface” are highlighted in green; in the repressed clusters, the terms “central nervous system

development", "positive regulation of epithelial cell proliferation" and "signaling pathways regulating pluripotency of stem cells" are highlighted in red. Note, the engraftable cultures are comprised by a mixture of cell phenotypes, which is reflected by the additional broad or non-neuronal GO terms identified here. This is consistent with the normal function of GBCs in vivo producing gland, duct and microvillar cells, in addition to neurons.

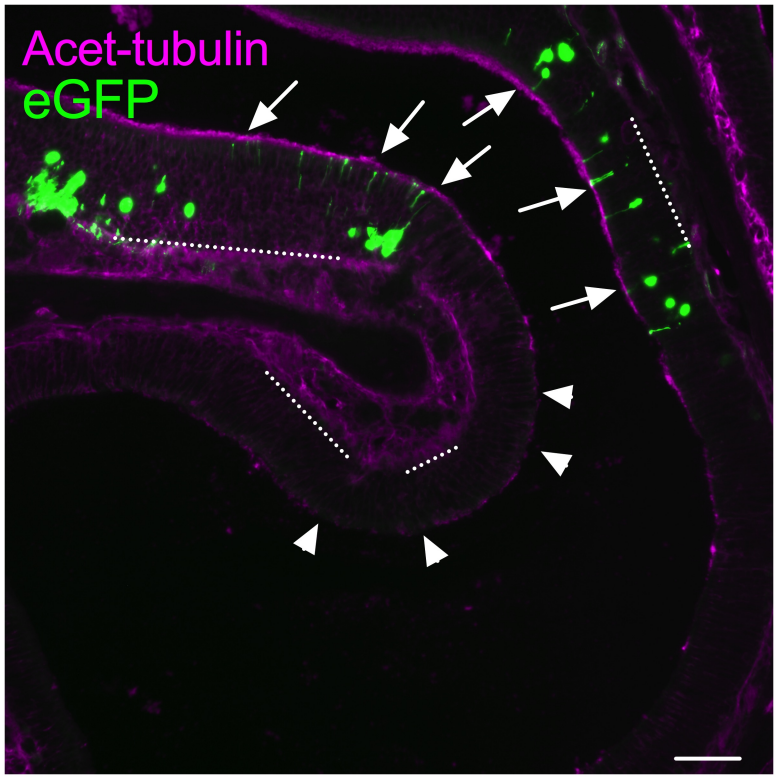

Figure S2. Additional example of cilia staining associated with engraftment-derived cells in the IH model. Representative tissue section from IH mouse 10 weeks following cell engraftment; staining of OE for acetylated tubulin (magenta) to label OSN cilia demonstrates cilia layer associated with dendritic knobs from eGFP^{+} engraftment-derived

cells (arrows). Cilia-deficient OE (arrowheads) lacks eGFP^{+} engraftment-derived neurons. Dashed lines mark basal lamina; bar 50 μm.

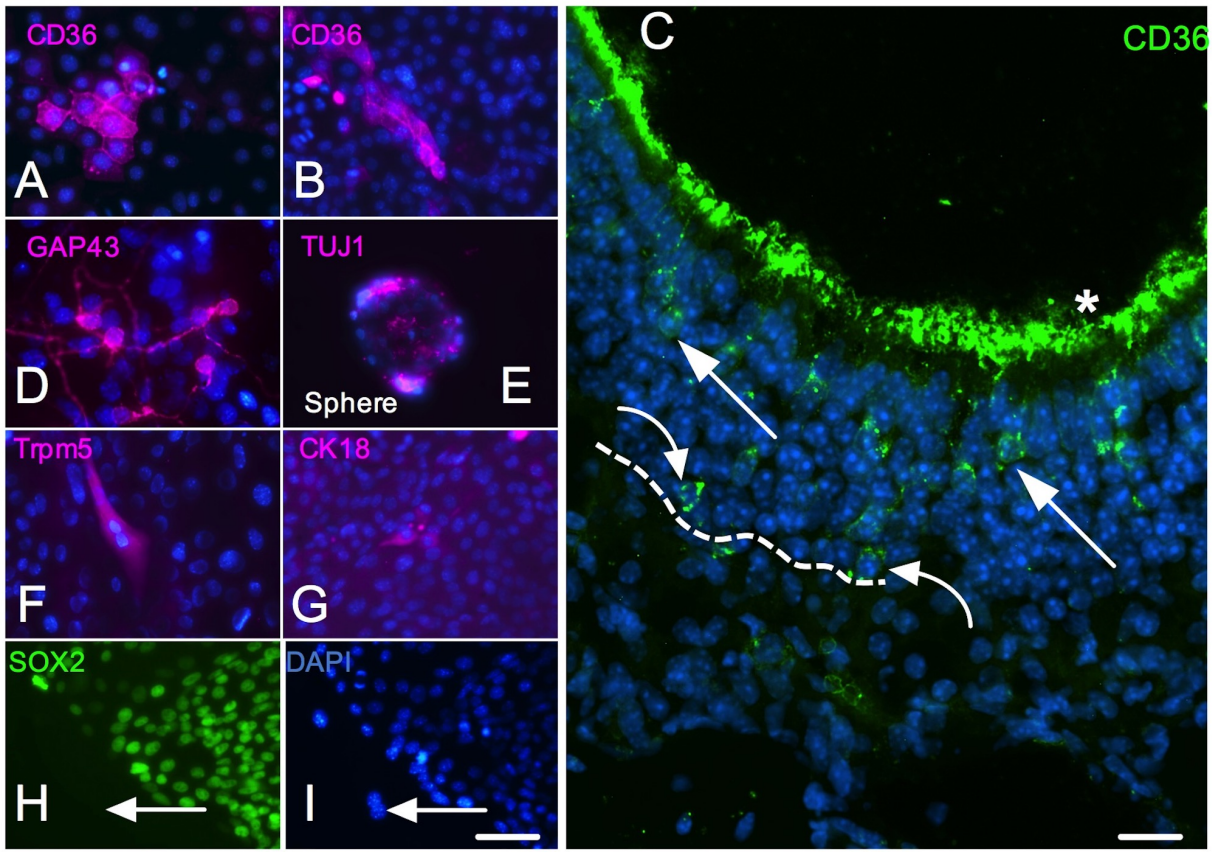

Figure S3. Immunocytochemical analysis of engraftable basal cell cultures. Culture morphology and RNA-seq results indicated that engraftment-competent cultures are heterogeneous, due to the presence of adherent islands, semi-adherent spheres, and differentiating migrating cells. We performed immunocytochemistry with available cell-type specific markers.

(A-C) RNA-seq identified the surface marker CD36 as highly enriched in engraftable cultures. We identify CD36 expression in a cell surface pattern among scattered clusters of adherent cells within culture islands (A, B), with an undifferentiated morphology. In tissue

sections, we identify CD36 expression in subsets of OSNs (C, straight arrows), where it has been reported to function as a volatile fatty acid receptor(Oberland et al., 2015; Xavier et al., 2016); however, we also identify CD36 expression in scattered basal layer cells (curved arrows), which has not been reported previously. Dashed line marks basal lamina in (C).

(D, E) The neuronal markers GAP43 and TUJ1 are widely expressed in cultures, largely in clusters of process-bearing cells migrating away from islands, or in the semi-adherent neurospheres.

(F) The microvillar cell marker Trpm5 is expressed infrequently in adherent cells with an elongated morphology.

(G) CK18, expressed in vivo by Bowman's glands, duct cells, and sustentacular cells, is also expressed infrequently among the adherent cell islands.

(H, I) SOX2 is widely expressed among adherent undifferentiated-appearing cells. While many cells are SOX2-bright, we identify heterogeneous expression, with obvious weakly-positive SOX2-low cells, as well as SOX2-negative cells (arrows), usually outside of the cell islands. In vivo, SOX2 is expressed in subsets of basal cells and in sustentacular cells, and SOX2 expression has been shown to be induced by injury among cells normally considered to be neuronal lineage basal cells (Lin et al., 2017). Bar 50 μm in A-I, except 25 μm in C.

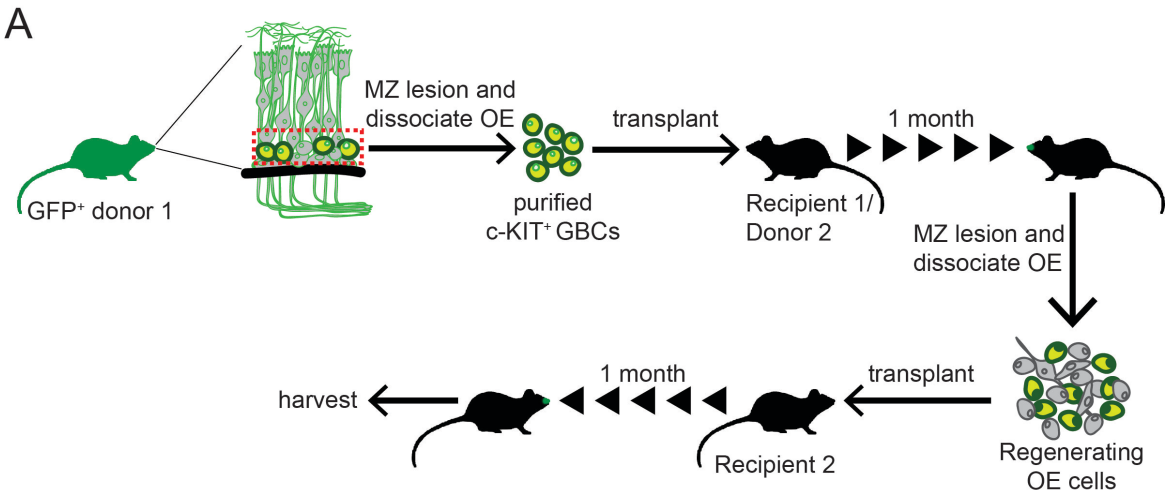

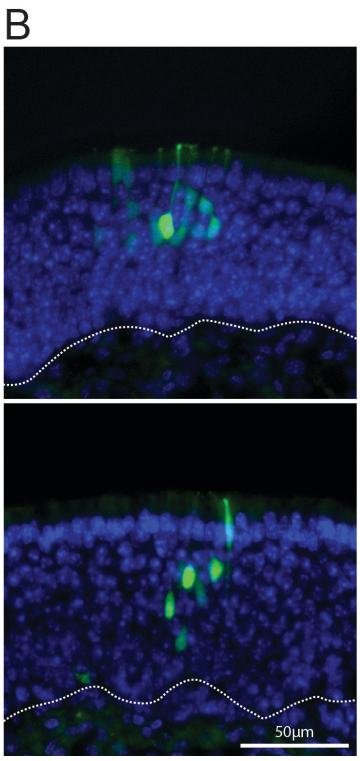

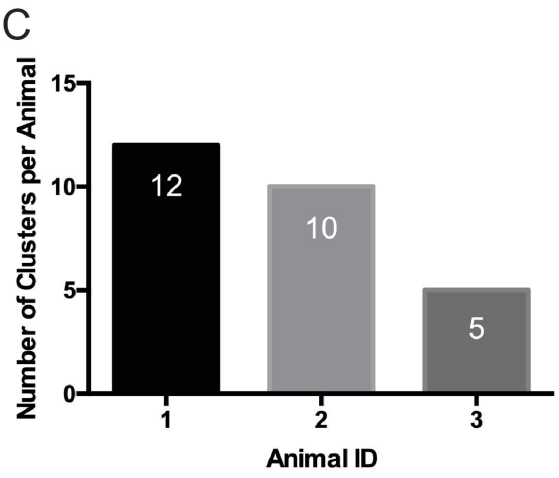

D

	Cell Types				
Animal ID	GBCs	Neurons	MV/Sus	Other	**Total**
1	4	58	7	2	**71**
2	5	33	7	0	**45**
3	2	0	5	0	**7**

Figure S4. Engraftment-derived basal cells possess serial repopulation potential. (A) Experimental design is shown. Following the same protocol used for engrafting purified c-KIT+ OE cells from regenerating eGFP+ donors, 9 wild type hosts were engrafted. After 1 month, the hosts were re-lesioned with methimazole, recovered 1 week, and dissociated OE cells were then harvested for engraftment into new wild type host mice. The second host mice (n=3) were euthanized after an additional 1 month recovery for analysis. (B)

Cryosections were examined to identify eGFP+ cell clusters within the OE. Examples shown here include olfactory neurons and a microvillar cell; nuclei are stained with DAPI, dashed line marks basal lamina, bar=50 μm. (C, D) Distinct cell clusters were quantified, and cell type assignments are shown. Although engraftment was sparse, these results provide direct evidence for the serial repopulating potential of engraftable basal cells, a classic definition of stemness.

SI References

Goldstein, B.J., Goss, G.M., Choi, R., Saur, D., Seidler, B., Hare, J.M., and Chaudhari, N. (2016). Contribution of Polycomb group proteins to olfactory basal stem cell self-renewal in a novel c-KIT+ culture model and in vivo. Development *143*, 4394-4404.

Lin, B., Coleman, J.H., Peterson, J.N., Zunitch, M.J., Jang, W., Herrick, D.B., and Schwob, J.E. (2017). Injury Induces Endogenous Reprogramming and Dedifferentiation of Neuronal Progenitors to Multipotency. Cell Stem Cell.

Livak, K.J., and Schmittgen, T.D. (2001). Analysis of relative gene expression data using real-time quantitative PCR and the 2(-Delta Delta C(T)) Method. Methods *25*, 402-408.

Oberland, S., Ackels, T., Gaab, S., Pelz, T., Spehr, J., Spehr, M., and Neuhaus, E.M. (2015). CD36 is involved in oleic acid detection by the murine olfactory system. Front Cell Neurosci *9*, 366.

Uhlen, M., Bandrowski, A., Carr, S., Edwards, A., Ellenberg, J., Lundberg, E., Rimm, D.L., Rodriguez, H., Hiltke, T., Snyder, M.*, et al.* (2016). A proposal for validation of antibodies. Nat Methods *13*, 823-827.

Xavier, A.M., Ludwig, R.G., Nagai, M.H., de Almeida, T.J., Watanabe, H.M., Hirata, M.Y., Rosenstock, T.R., Papes, F., Malnic, B., and Glezer, I. (2016). CD36 is expressed in a defined subpopulation of neurons in the olfactory epithelium. Sci Rep *6*, 25507.